ACSNANO

www.acsnano.org

ARTICLE

Near Infrared-Guided Smart Nanocarriers for MicroRNA-Controlled Release of Doxorubicin/siRNA with Intracellular ATP as Fuel

Penghui Zhang,[†,§] Chen Wang,[‡,§] Jingjing Zhao,[†] Anqi Xiao,[†] Qi Shen,[†] Linting Li,[†] Jianxin Li,[†] Junfeng Zhang,[‡] Qianhao Min,[*,†] Jiangning Chen,[*,‡] Hong-Yuan Chen,[†] and Jun-Jie Zhu[*,†]

[†]State Key Laboratory of Analytical Chemistry for Life Science, School of Chemistry and Chemical Engineering, Nanjing University, Nanjing 210093, P. R. China

[‡]State Key Laboratory of Pharmaceutical Biotechnology, Jiangsu Engineering Research Center for microRNA Biology and Biotechnology, School of Life Sciences, Nanjing University, Nanjing 210093, P. R. China

Supporting Information

ABSTRACT: **In chemotherapy, it is a great challenge to recruit endogenous stimuli instead of external intervention for targeted delivery and controlled release; microRNAs are the most promising candidates due to their vital role during tumorigenesis and significant expression difference. Herein, to amplify the low abundant microRNAs in live cells, we designed a stimuli-responsive DNA Y-motif for codelivery of siRNA and Dox, in which the cargo release was achieved *via* enzyme-free cascade amplification with endogenous microRNA as trigger and ATP (or H^+) as fuel through toehold-mediated strand displacement. Furthermore, to realize controlled release in tumor cells, smart nanocarriers were constructed with stimuli-responsive Y-motifs, gold nanorods, and temperature-sensitive polymers, whose surfaces could be reversibly switched between PEG and RGD states *via* photothermal conversion. The PEG corona kept the nanocarriers stealth during blood circulation to protect the Y-motifs against nuclease digestion and enhance passive accumulation, whereas the exposed RGD shell under near-infrared (NIR) irradiation at tumor sites facilitated the specific receptor-mediated endocytosis by tumor cells. Through modulating NIR laser, microRNA, or ATP expressions, the therapy efficacies to five different cell lines were finely controlled, presenting NIR-guided accumulation, massive release, efficient gene silence, and severe apoptosis in HeLa cells; *in vivo* study showed that a low dosage of nanocarriers synergistically inhibited the tumor growth by silencing gene expression and inducing cell apoptosis under mild NIR irradiation, though they only brought minimum damage to normal organs. The combination of nanomaterials, polymers, and DNA nanomachines provided a promising tool for designing smart nanodevices for disease therapy.**

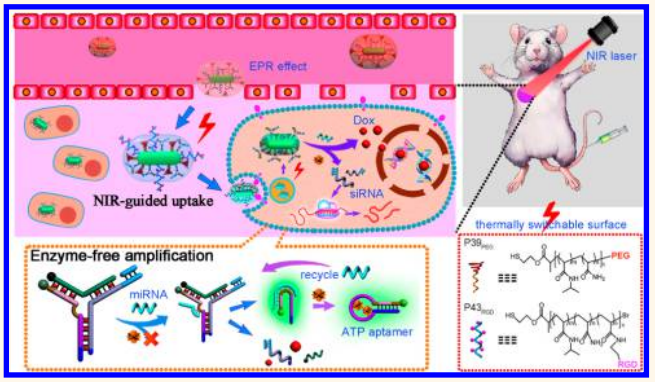

KEYWORDS: *microRNA, aptamer, DNA nanomachine, smart nanocarriers, drug delivery*

Smart stimulus-responsive nanocarriers for cancer therapy have gained considerable attentions in recent years. Materials including liposomes, polymers, micelles, and inorganic particles are selected as potential candidates to construct these smart nanocarriers.[1−6] Meantime, many triggering stimuli are explored for the smart nanocarriers, including external signals, such as temperature,[7] light,[8] magnetic field,[9] and ultrasound,[10] as well as physiological factors, such as pH,[11] redox potential,[12] and enzymes and biomolecules.[13,14] The active targeting and stimuli-responsive characteristics of smart nanocarriers have facilitated their specific accumulation at tumor sites and controlled release in target cells, which is beneficial to tailor pharmacokinetics, enhance therapy efficacy, and alleviate side effects. Nevertheless, the high similarity in microenvironment between tumor and peripheral normal tissues makes them hard to achieve exclusive cellular uptake and discrepant release in tumor cells.

MicroRNA (miRNA) is a promising endogenous stimulus, as well as a potential therapeutic target because it shows considerable differential expression between the malignant tissues and their normal counterparts.[15] However, due to their low amounts,[16] usually less than 50 000 copies per cell, the drug

Received: December 25, 2015
Accepted: February 23, 2016
Published: February 23, 2016

DOI: 10.1021/acsnano.5b08145
ACS Nano 2016, 10, 3637−3647

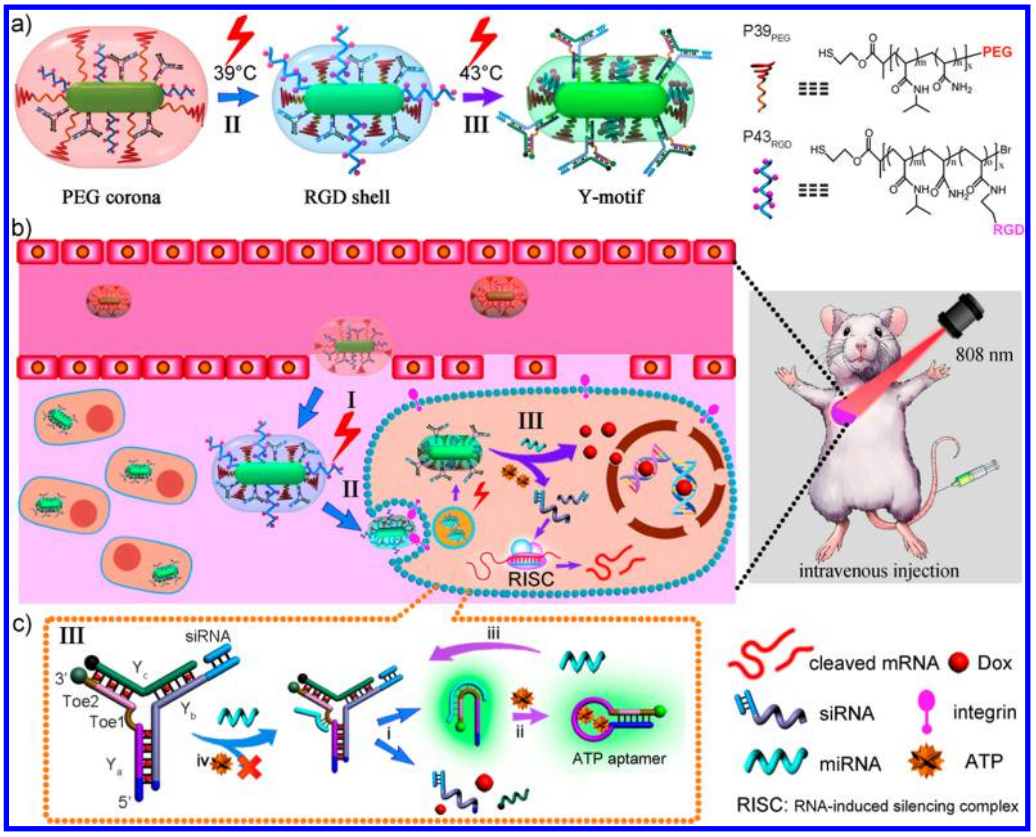

Figure 1. Schematic design of the smart nanocarriers triggered by miRNA and fuelled by ATP. (a) Thermal-responsive regulation of the surface composition. (b) NIR-guided delivery and controlled release *in vivo*. I, passive accumulation at tumor sites *via* EPR effect; II, specific uptake *via* receptor-mediated endocytosis; III, controlled release by endogenous miRNA/ATP. (c) Amplified dissociation of Y-motifs based on TMSD cascade reactions with miRNA as trigger and ATP as fuel: i, Toe1-TMSD triggered by miRNA; ii, ATP (or H^+) recognition by aptamer; iii, Toe2-TMSD for miRNA regeneration.

release triggered by miRNAs was greatly hindered.[17] The novel strategies should be developed in order to utilize the trace intracellular miRNAs as stimuli. Although masses of methods have been developed for gene segment analysis *via* enzymatic amplification techniques, such as polymerase chain reaction, rolling circle amplification, and ligase chain reaction,[18] it remains a great challenge to reconstruct the enzymatic amplification in situ by delivering the enzymes and their substrates into live cells simultaneously.[19] Recently, emerging evidence show that toehold-mediated strand displacement (TMSD), activated by initiator DNA strands and powered by fuelling strands *via* free-energy-driven hybridization, is an efficient enzyme-free amplification reaction for catalytic labels and target regeneration, particularly applied in molecular machines, catalytic circuits, and logic gates.[20−24] More excitingly, besides the classical double helix, formation of G-quadruplex or i-motif structures can also activate the TMSD reactions,[25] making it possible to design DNA nanomachines to realize in situ amplification of gene targets in live cells. In this study, to recycle the trace intracellular miRNAs, an enzyme-free amplification strategy based on TMSD was developed using ATP and H^+ as intracellular fuels; the designed DNA Y-motif also served as scaffolds to carry the doxorubicin (Dox) at GC base pairs, whereas the drugs were eventually released through three cascade processes (Figure 1c).

During chemotherapy, many cancer cells develop defensive strategies against the chemotherapy-induced death by up-regulating antiapoptosis pathways, altering cell cycle checkpoints or increasing repair mechanism.[26] To address this issue, small interference RNA (siRNA), which can disrupt cellular pathways by knocking down gene expressions, has been combined with chemotherapy to silence the antiapoptotic genes and sensitize the cells to drugs.[27] When the nuclease degradation and renal clearance during siRNA delivery is considered, numbers of nanocarriers were developed with PEG conjugation as a common strategy to extend blood circulation and increase passive accumulation at tumor sites by enhanced permeability and retention (EPR) effect, which in turn weakened cellular uptake.[28,29] In order to solve this dilemma, sheddable PEG coronas responsive to specific stimuli, such as decreased pH, overexpressed enzymes, or hypoxia microenvironment were designed to change the surface states to realize specific cellular uptake when the nanocarriers arrived at tumor tissues *via* EPR effect.[30−32] Thermosensitive polymers, undergoing reversible phase transition from hydrophilic to hydrophobic state at lower critical solution temperature (LCST),[33,34] provide a promising way to reversibly adjust the surface composition of the nanocarriers, thereby allowing selective cell entry in a controlled manner.

Herein, the smart nanocarriers with thermally switchable surface were constructed by assembling stimuli-responsive Y-motifs and two thermosensitive polymers (PEG tailed $P39_{PEG}$ with LCST at 39 °C and RGD conjugated $P43_{RGD}$ with LCST at 43 °C) onto the surface of gold nanorods (GRs) for codelivery of siRNA and Dox *in vivo* for cancer therapy (Figure 1). Specific siRNA targeted to polo-like kinase 1 (PLK1) was coupled at the end of the Y-motif scaffold, whereas Dox was intercalated into the GC base pairs. Particularly, below 39 °C,

DOI: 10.1021/acsnano.5b08145
ACS Nano 2016, 10, 3637−3647

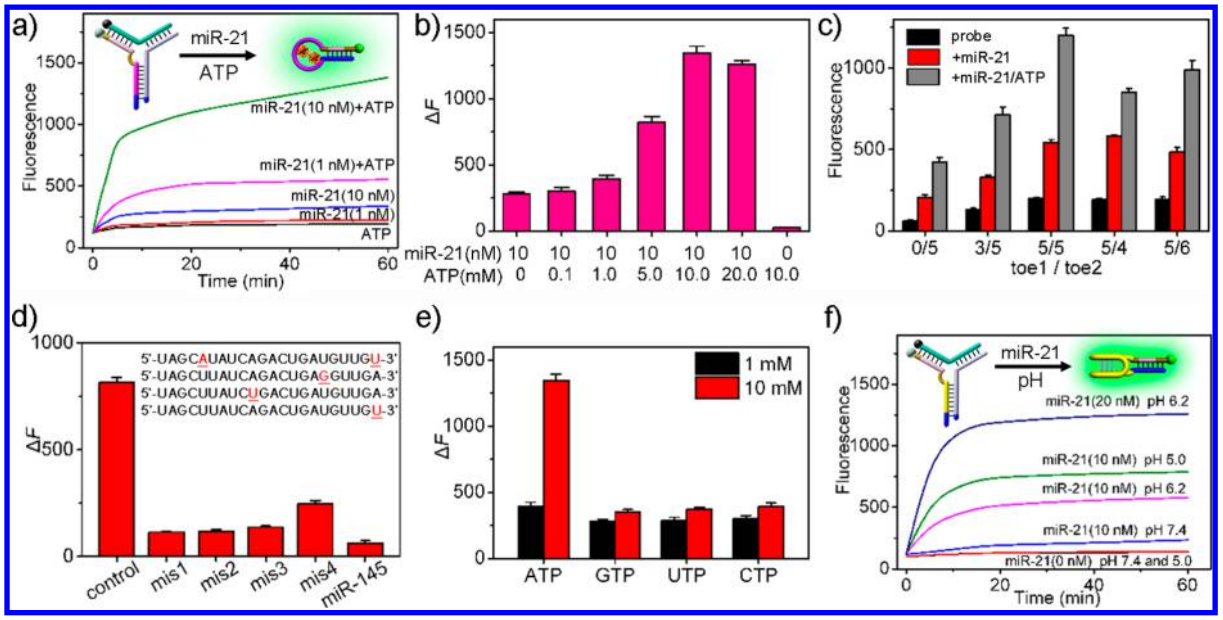

Figure 2. Design of miRNA-responsive Y-motifs respectively fuelled by ATP and acidic pH. (a) Fluorescence experiments of the Y-motif nanoprobes (1 μM) in the presence of different concentrations of miR-21 and ATP. (b) Effects of the ATP concentration on the strand displacement kinetics. (c) Effects of the toehold length on the cascade reactions. (d) Discrimination of the nanoprobes to mismatched miR-21. (e) Fluorescence variations of the nanoprobes (1 μM) containing 10 nM miR-21 in the presence of ATP, GTP, UTP, and CTP. (f) Effects of the pH values on the strand displacement kinetics of the Y'-motif incorporated with i-motif (1 μM). All the error bars indicate s.d. (n = 3) and all the fluorescence signals were recorded at 520 nm with excitation at 485 nm.

the smart nanocarriers' surfaces were dominated by PEG corona, which helped to protect the coupled Y-motifs from nuclease degradation and renal clearance after intravenous injection and favored their accumulation at tumor sites *via* EPR effect. Under mild near-infrared (NIR) irradiation, the gold nanorods heated the surrounding over 39 °C, leading to the shrinkage of $P39_{PEG}$ and the exposure of $P43_{RGD}$, thereby enhancing the uptake by tumor cells *via* receptor-mediated endocytosis.[35] After cellular uptake, with the further increase of NIR laser power, the outmost surface composition of smart nanocarriers switched from RGD to Y-motifs with the curling of $P43_{RGD}$. Then, the nanocarriers rapidly escaped from the endosome into cytosol, where the endogenous miRNAs triggered the dissociation of the Y-motifs in the presence of ATP, thereby releasing the loaded Dox and siRNA, which synergistically induced cell apoptosis and inhibited tumor growth. The smart nanocarriers explored a promising approach for cancer therapy combined with gene and drugs in a controlled manner.

RESULTS AND DISCUSSION

Design of DNA Nanomachines Responsive to miRNAs with ATP or H^+ as Fuel. The amplification strategy was depicted in Figure 1c and Figure S1. Through rational DNA design, a complementary segment to miRNA and an ATP aptamer were stapled in a Y-shaped DNA hybrid termed as Y-motif, where the binding of aptamer to ATP was completely sequestered due to the duplex hybridization; meanwhile, the Y-motif provided convenient scaffold for siRNA coupling and sufficient sites for Dox loading. In step i, the miRNAs attached on the unpairing domain of Toe1 at Y_a to initiate the strand displacement reaction, resulting in the liberation of aptamer from the rigid Y-motif. The tertiary structure of the liberated aptamer was switched from metastable duplex to stable hairpin along with the specific binding to ATP, leading to the collapse of Y-motif and cargo release in step ii. In step iii, the energy-favored hairpin structure promoted the approach of the sticky 5′ end to the unpaired overhang at Toe2, where Toe2-mediated strand displacement occurred to regenerate the miRNAs from Y_a strand; the released miRNAs would autonomously move to the neighboring Y-motifs for further hybridization, thus generating a continuous drug release.

To verify the proposed recycle strategy, a fluorescence turn-on probe was constructed by labeling the fluorophore FAM and quencher BHQ at the ends of Y_a and Y_c, respectively. First, stoichiometric amounts of strands Y_a, Y_b, and Y_c were mixed in Tris−HCl buffer; the resulting solution emitted weak background fluorescence due to the close proximity of FAM and BHQ in the Y-motif. With the addition of 1 nM miR-21, the fluorescence had a gradual recovery, which was attributed to the miRNA-triggered and Toe1-mediated one-to-one strand displacement; in contrast, once exposed on 10 mM ATP (a typical concentration in cytosol),[14,36] the fluorescence probes exhibited a rapid response to miR-21 in a concentration-dependent manner (Figures 2a and S2), indicating that the conformation switching of the aptamer induced by ATP recognition had efficiently promoted the Toe2-mediated strand displacement, leading to the recycling of miR-21 in the enzyme-free nucleic acid-activated cascade reactions.[37] Meanwhile, Figure 2b revealed that the strand displacement kinetics were finely controlled by varying the concentrations of ATP; thus, the miRNA-triggered multistep TMSD reactions were efficiently enhanced with the fueling of ATP in the range between 5 mM and 20 mM. Furthermore, the effects of toehold length on the amplification kinetics were investigated. As predicted, increasing the length would favor the displacement reaction. However, considering the stability of the Y-shaped structure and the kinetics of the whole strategy, the lengths of Toe1/Toe2 were optimized to be 5/5 in Figure 2c. In addition, the discrimination of the probes was explored that only the

DOI: 10.1021/acsnano.5b08145
ACS Nano 2016, 10, 3637−3647

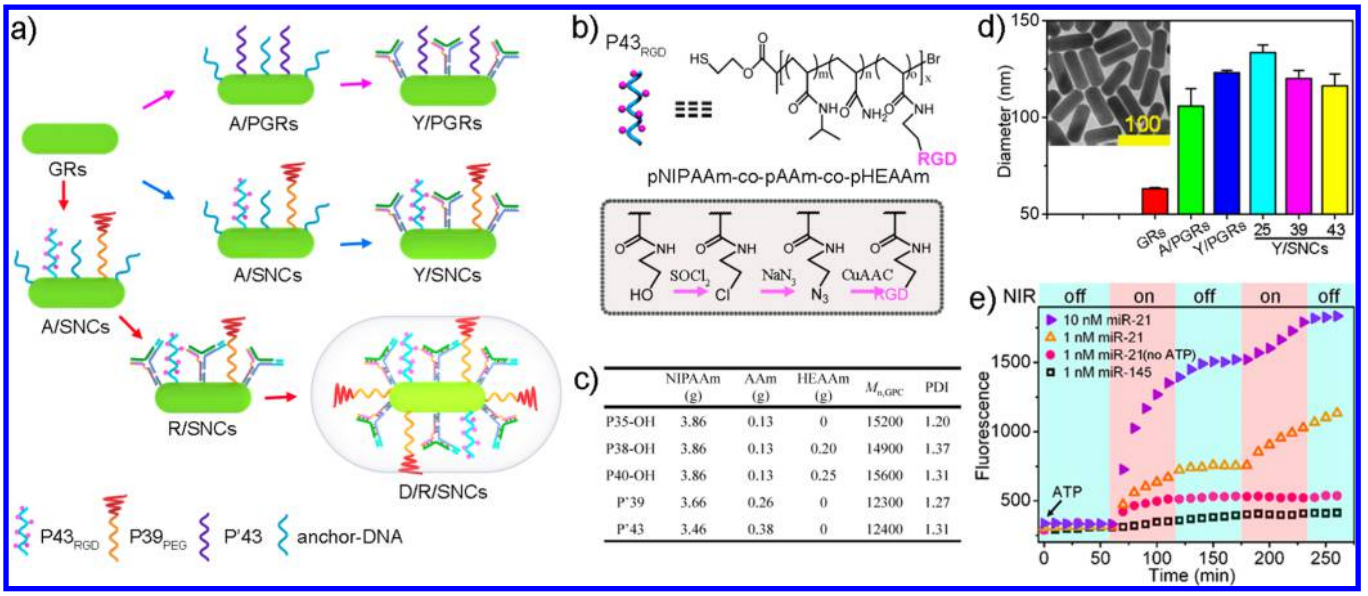

Figure 3. Characterization of miRNA/ATP-responsive nanocarriers. (a) Schematic illustration of the preparation of different nanocomposites. (b) Functionalization procedures of $P43_{RGD}$. (c) Properties of the synthesized polymers. (d) DLS data of GRs, A/PGRs, Y/PGRs, Y/SNCs. Inset is the TEM images of GRs. (e) Time-dependent Dox fluorescence variations of D/R/SNCs (10 nM) in Tris−HCl buffers with the addition of miRNAs and ATP. The solutions were exposed under NIR laser with the power density of 0.5 W cm^{-2}. During the measurement, the laser was repeatedly turned on and off, and the Dox fluorescence in the solution was recorded with emission at 590 nm and excitation at 485 nm.

perfect hybridization of the Y-motif with its target triggers and fuels could efficiently initiate the cascade amplification, whereas any mismatch, even at the terminus of the sequence, would drastically reduce the reaction rates, implying the high selectivity of our probes in distinguishing miRNA family with high sequence homology (Figure 2d), as well as NTP analogues (GTP, UTP, and CTP in Figure 2e).

Most importantly, to testify the versatility of our DNA nanomachine, another amplification strategy was developed with miRNA as trigger and H^+ as fuel by replacing the ATP aptamer with a cytidine-rich oligomer (known as i-motif). Similarly, the sensitive response of i-motif to pH changes was completely sequestered in the Y-motif until the miRNA initiated the Toe1-mediated displacement. As shown in Figure 2f, the exposed i-motif maintained the duplex with Y_b in neutral solution; when the pH value was lowered, the cytosine became partially protonated, leading to the structure transformation to DNA tetraplex,[38] which accelerated the following Toe2-mediated strand displacement. Meantime, the multistep cascade amplification also exhibited concentration-dependent characteristic, pH-controlled reaction kinetics (Figure S3a), and high selectivity to mismatched miRNA mimics (Figure S3b), setting an ideal model for the design of stimuli-responsive DNA nanodevices.

Preparation of the Smart Nanocarriers for Codelivery of siRNA and Dox. Next, to avoid the nuclease digestion during delivery and enhance the uptake by target cells, smart nanocarriers with thermally tunable surface were constructed by assembling the stimuli-responsive Y-motifs and two temperature-responsive polymers onto the surface of GRs (Figure 3a). As characterized in Figures 3b, c, and S4−S5, $P39_{PEG}$ and $P43_{RGD}$ were obtained by adjusting the monomer compositions to control the molecular weight, conjugation density, and LCST. Interestingly, the increasing densities of functionalized molecules significantly impacted the temperature sensitivity of the polymer, especially resulting in a higher LCST at 43 °C in $P43_{RGD}$ with an estimated density of 16 RGD motifs per chain compared with its precursor P40-OH. Then the two polymers were covalently anchored on GRs with thiol-ended anchor-DNA at an optimized molar ratio of 2:1:3 to replace the CTAB surfactants (Figure S6), which were confirmed by dynamic light scattering (DLS, Figure 3d), UV−vis spectra (Figure S7), and zeta potential (Figure S8). The DLS data confirmed that with the PEG conjugation, Y/SNCs had a larger hydrodynamic diameter than Y/PGRs, meaning that $P39_{PEG}$ has formed a PEG corona around the nanocarriers. With the temperature increasing, the multiple thermal-responses of the Y/SNCs were directly reflected by the continuous decreases of diameters at 39 and 43 °C, corresponding to the sequential curling of the $P39_{PEG}$ and $P43_{RGD}$. Though loading Dox and siRNA in the Y-motifs, the smart nanocarriers of D/R/SNCs were prepared with estimated loading capacity of 112 siRNA copies and 3000 Dox molecules per nanoparticle (Figure S9).[14,39] Subsequently, the release of the cargos was spatial-temporally controlled by the modulation of the NIR light, miRNA, and ATP in Figure 3e. The fluorescence of Dox (Figure S10) is completely quenched after intercalation in the GC pairs on the nanocarriers due to fluorescence resonance energy transfer (FRET), but it presents a turn-on behavior in response to its target miRNA, which is favorable for visualizing drug release in real time. At the room temperature of 25 °C, the response function of the Y-motifs was totally sequestered due to the steric hindrance by the PEG corona. As expected, upon the NIR irradiation, the GRs in the core heated the surroundings *via* photothermal effect, leading to the shrinkage of polymers and exposure of Y-motifs, where the cascade amplification reaction was reinitiated in the presence of miRNA and ATP; the dissociation of the DNA nanostructures elicited the cargo release with a burst increase in Dox fluorescence. Consequently, in the presence of 10 mM ATP, 1 nM miRNAs completely dissociated 100-fold Y-motifs on the nanocarriers in 4 h under the NIR irradiation, leading to the release of 60%

DOI: 10.1021/acsnano.5b08145
ACS Nano 2016, 10, 3637−3647

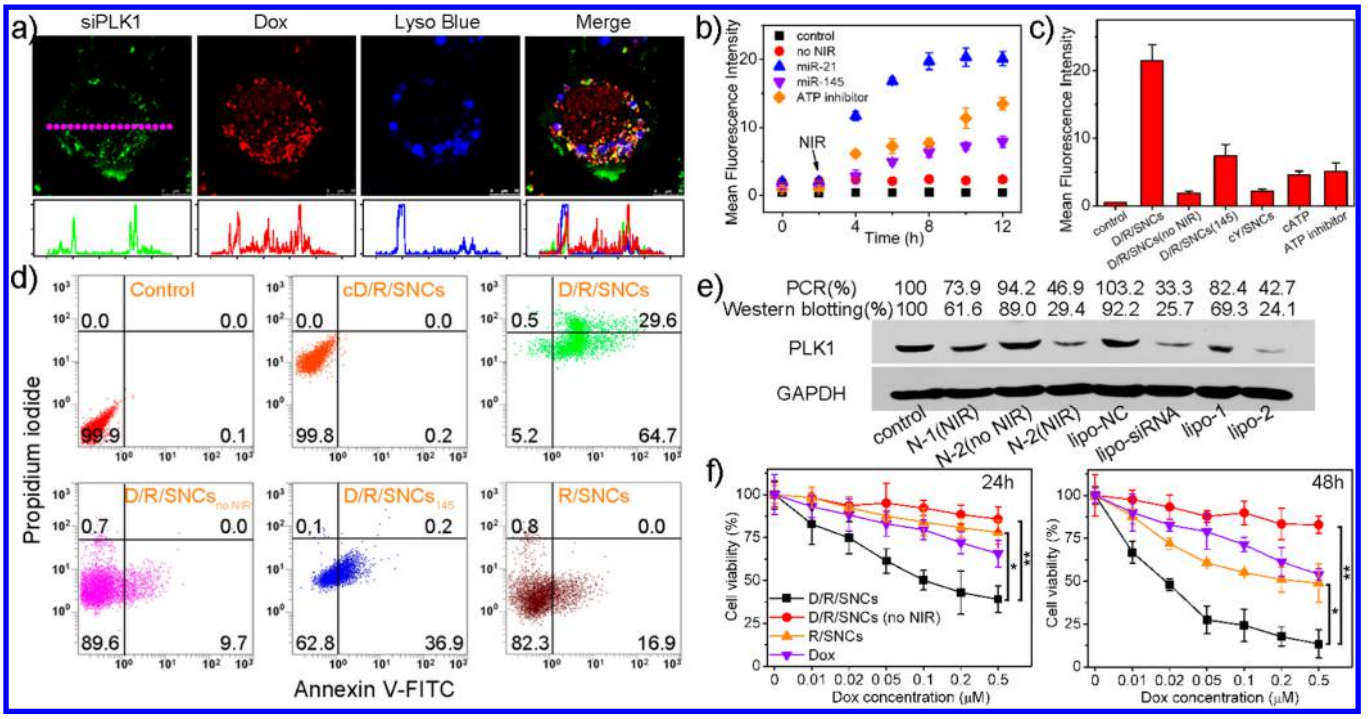

Figure 4. NIR-guided delivery and miRNA/ATP-controlled release *in vitro*. (a) Confocal images of HeLa cells after incubation with D/R/SNCs for 6 h. The green fluorescence comes from the FAM labeled siPLK1, whereas the red from the Dox molecules. (b) The controlled release of Dox in HeLa cells. (c) Mean fluorescence intensity of Dox in HeLa cells after incubation with different nanocarriers. In the control group of cY/SNCs (or cATP), the corresponding DNA segment interacting with miRNA (or ATP) was replaced with random sequences. (d) Flow cytometric analysis of HeLa cell apoptosis after incubation with different nanocarriers for 12 h using Annexin V-FITC/PI staining. The group of cD/R/SNCs was set as positive control in which the cells were treated with D/R/SNCs under NIR laser, but not stained with the apoptotic kit. (e) Relative PLK1 mRNA levels measured by qRT-PCR and PLK1 protein expression levels evaluated by Western blotting after delivery of siRNA by R/SNCs into the HeLa cells. siPLK1-1 and siPLK1-2 were respectively delivered by nanocarriers (N-1, N-2) and Lipofectamine (lipo-1, lipo-2). Nonsense siRNA was selected as the negative control (lipo-NC). (f) Cell viability in HeLa cells after incubation with different formulations for 24 and 48 h. To simplify the comparison, the group of R/SNCs has the same particle concentration with the group of D/R/SNCs. Error bars indicate s.d. (n = 4). *P < 0.05, **P < 0.01 (two-tailed Student's t-test).

Dox molecules and 90% siRNAs into the bulk solution. Finally, it should be noted that the DNA coating and PEG protection had significantly enhanced the stability of the nanocarriers, thus presenting excellent colloidal stability in saline and cultured medium against nonspecific adsorption, acid degradation, and nuclease digestion by DNase I and RNase A (Figure S11), as well as reversible response to temperature variations (Figure S12), providing a promising candidate for delivering siRNAs and Dox *in vivo*.

NIR-Guided Target Delivery and Controlled Drug Release of the Smart Nanocarriers *In Vitro*. In cancer treatment, Polo-like kinase 1 (PLK1), a highly conserved serine−threonine kinase that promotes cell division, is an attractive therapeutic target in that it is overexpressed in diverse cancer types, whereas suppressing its expression with small interfering RNA (siPLK1) leads to cell cycle arrest, apoptosis, and mitotic catastrophe. More importantly, the combination of siPLK1 with anticancer drugs remarkably inhibited the tumor growth and metastasis in a synergistic manner.[40] In this case, siPLK1 were loaded with Dox in the smart nanocarriers, which showed high biocompatibility to cells due to the complete elimination of CTAB molecules by ligand exchange (Figure S13). The effects of the NIR irradiation on cell uptake and cargo release were quantified by determining the gold amounts with ICP-MS and visualized by recording the Dox fluorescence with flow cytometry (Figure S14). Upon the NIR irradiation, the uptake amounts drastically increased with the increase of laser power, suggesting that the PEG corona around the nanocarriers has hindered their cellular uptake, whereas the exposure of RGD shell resulted in the specific recognition to integrin and subsequent receptor-mediated endocytosis; on the contrary, the further increase in laser power deteriorated the cellular uptake due to the shrinkage of $P43_{RGD}$. After internalized into cells, it was exciting to find that the release of Dox was also impacted by the NIR irradiation with a fast release in 2 h. The confocal images in Figure 4a suggested that both the siPLK1 and Dox released from the nanocarriers had a poor correlation with the endosome/lysosome stained by Lyso blue, indicating that the nanocarriers had successfully escaped from the endosome into cytosol, where the cargo release was triggered by endogenous miRNAs in ATP-rich environment. The role of NIR light in the rapid endosome escape was further explored by monitoring the fluorescence variations of the endosome. The decaying and shapeless blue fluorescence under NIR irradiation (Figures S14c−d) reflected that the photothermal heating might disrupt the endosome and facilitate the escape of the nanocarriers into cytosol,[41] which were also confirmed by the TEM images in Figure S15 that masses of nanocarriers uniformly distributed in the cytosol, whereas a few remained in the endosome. Thus, by adjusting the NIR power, the surface state of the nanocarriers could be finely tuned, which directly affected the cell uptake and intracellular trafficking.

DOI: 10.1021/acsnano.5b08145
ACS Nano 2016, 10, 3637−3647

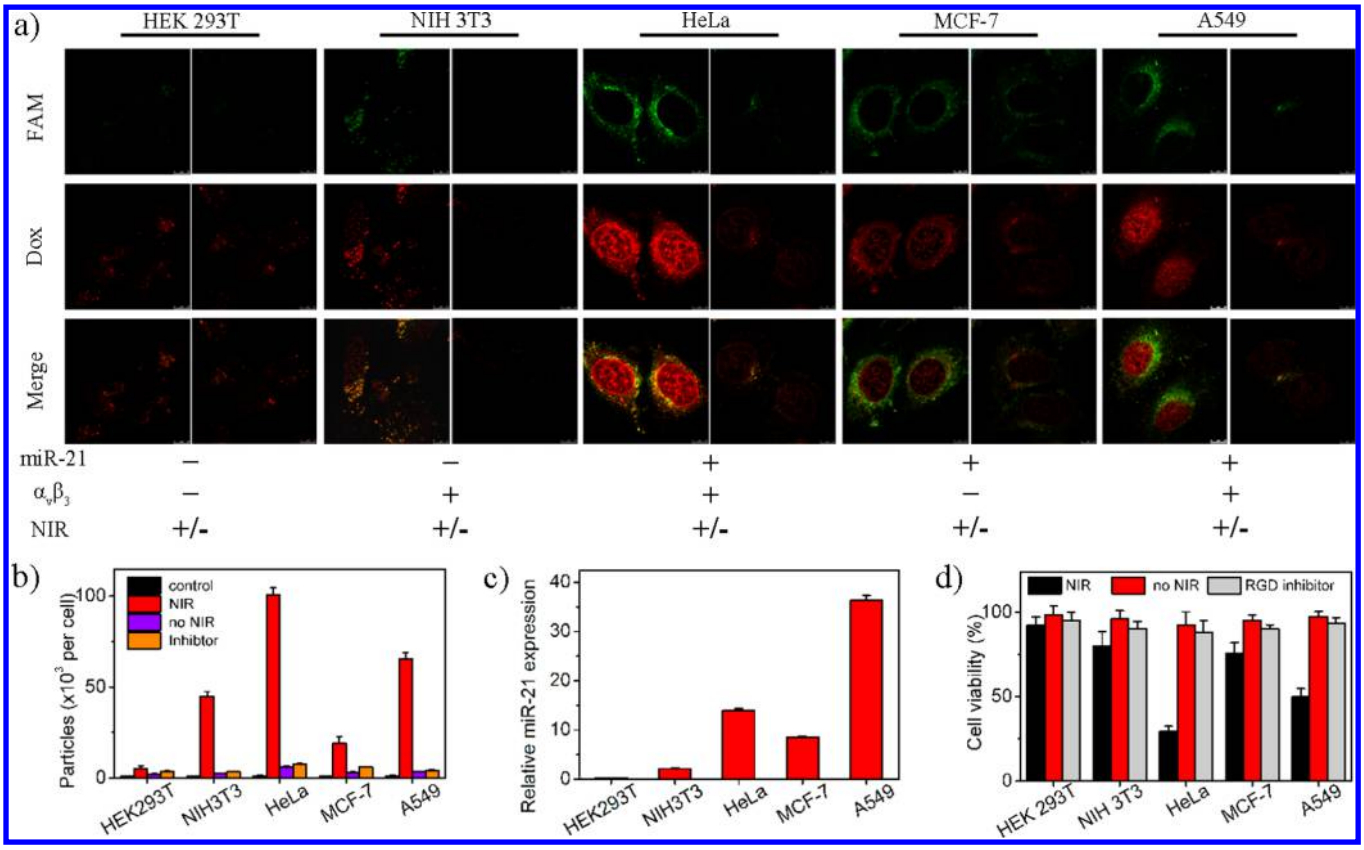

Figure 5. Therapeutic efficacy of the smart nanocarriers to different cell lines. (a) The confocal images of HEK 293T, NIH 3T3, HeLa, MCF-7, and A549 cells after incubation with D/R/SNCs under NIR irradiation (+) or not (−). The green fluorescence comes from the FAM labeled siRNA and the red color from Dox. (b) Cellular uptake efficiency of the nanocarriers in HEK 293T, NIH 3T3, HeLa, MCF-7, and A549 cells. (c) Relative expressions of miR-21 in five different cell lines. (d) Cell viability of the five different cells with the treatment of the nanocarriers. All the error bars indicate s.d. (n = 3).

Besides NIR regulation, the release of the cargo from the nanocarriers could also be controlled by altering the expressions of miRNA and ATP inside the cells. As shown in Figures 4b and c, the overexpressed miR-21 in HeLa cells triggered a faster Dox release compared with miR-145, leading to a larger fluorescence accumulation and enhanced cytotoxicity. However, by virtue of the ATP-fuelled amplification, low-abundant miR-145 still could trigger considerable Dox release in a prolonged time and induce a continuous mortality to HeLa cells. Furthermore, the therapy efficacy could be subtly adjusted by combining the nanocarriers with gene therapy *via* the transfection of miRNA mimics or inhibitors into cells. The introduction of miRNAs drastically accelerated the TMSD-mediated amplification and resulted in intensified cytotoxicity (Figure S16); conversely, the inhibitor strands obviously reduced the miR-21 concentration and efficiently blocked the drug release, contributing to high cell viability. When replacing the Y-motifs with random DNA sequences, no signal amplification was observed in the nanocarriers of cY/SNCs and cATP in Figure 4c. Additionally, the role of intracellular ATP in drug release was testified by inhibiting the ATP production in cytosol with a chemical inhibitor iodoacetic acid (Figure S17); the decrease of ATP showed great impact on the release rate. Overall, the modulation of NIR-irradiation power, miRNA expression, and ATP concentration is an effective means to spatially and temporally control the drug release rates.

Furthermore, the roles of siPLK1 and Dox during the combination therapy were elucidated by Annexin V-FITC/PI apoptosis detection. The flow cytometric results in Figure 4d displayed that the apoptosis exhibited a direct correlation with the intracellular abundance of different triggers. Compared with miR-145, the total apoptotic ratio of D/R/SNCs responsive to miR-21 was up to 94.3%. This apoptotic ratio was also much higher than 16.9% of R/SNCs, which indicated that the combination of gene silence and Dox intercalation had induced the tumor cells into more severe apoptosis than gene therapy alone. The knockdown of PLK1 was testified by detecting the levels of PLK1 mRNA and protein after respectively incubating with the nanocarriers for 24 and 48 h. As shown in Figure 4e, with the aid of NIR laser, the nanocarriers feasibly entered the HeLa cells, escaped from the endosome, released the siPLK1 into cytoplasm, and knocked down the PLK1 protein to 29.4% (N-2), which was similar to the effect of transfecting ~10-fold free siPLK1 with commercial Lipofectamine 2000 (lipo-siRNA) and much more efficient than that of other formulations. It should be noted that the coupling position of siRNA on DNA scaffold showed a great impact on its silence function; in this case, coupling the DNA sequence at the 3′ end of the sense strand (N-2) presented a higher knockdown efficiency than that at the antisense strand (N-1). Finally, the therapy efficacy of the nanocarriers was checked by MTT assay. Different from Dox and R/SNCs (Figure 4f), 20 pM D/R/SNCs containing 0.05 μM Dox has caused more than 70% cell death at 48 h with a combination index (CI) less than 1, suggesting a synergistic effect of siPLK1 and Dox in inhibiting tumor cell growth.[42] Taken together, under the regulation of NIR power, miRNA

DOI: 10.1021/acsnano.5b08145
ACS Nano 2016, 10, 3637−3647

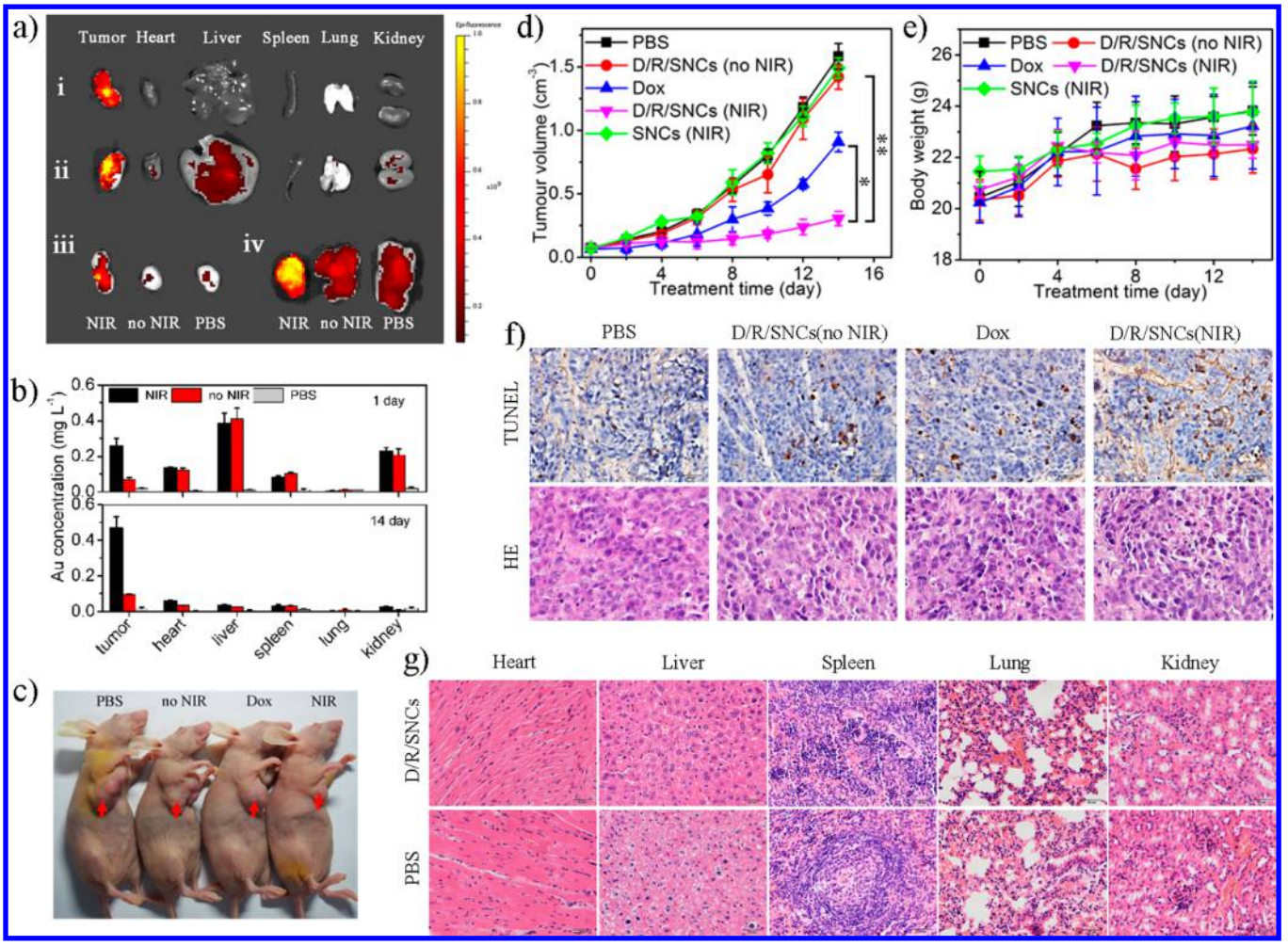

Figure 6. Tumor targeting and antitumor efficiency. (a) *Ex vivo* fluorescence imaging of the tumor and normal tissues harvested from the euthanized mice under NIR irradiation at (i) Day 1 and (ii) Day 14. The tumors came from different groups at (iii) Day 1 and (iv) Day 14. The fluorescence attributed to the released Dox was captured with excitation at 485 nm. (b) Biodistribution of the nanocarriers in the nude mice at Day 1 and Day 14. (c) Representative images of the xenograft tumors in mice after treatment with different nanocarriers at Day 14. (d) Tumor growth curves after intravenous injection of different formulations. Error bars indicate s.d. (n = 5). *P < 0.05, **P < 0.01 (two-tailed Student's t-test). (e) Body weight variation of tumor-bearing mice during treatment. Error bars indicate s.d. (n = 5). (f) TUNEL and histological observations to assess the apoptosis of the tumor tissues after treatment. (g) Histological observation of the normal tissues after treatment.

and ATP concentrations, D/R/SNCs could simultaneously deliver and release siPLK1 and Dox into the tumor cells in a finely controlled manner, exerting a synergistic impact on apoptosis induction.

Manipulating the Cytotoxicity of D/R/SNCs against Different Cells. The switchable surface of D/R/SNCs under NIR irradiation facilitated the reversible interaction between the nanocarriers and the HeLa cells, making it possible to regulate the cellular uptake on command. In order to further test the controllability in cell uptake, the nanocarriers were incubated with two integrin $\alpha_v\beta_3$-negative ($\alpha_v\beta_3^-$) cells of HEK 293T and MCF-7, and three integrin $\alpha_v\beta_3$-positive ($\alpha_v\beta_3^+$) cells of HeLa, A549, and NIH 3T3.[43−45] Cellular uptake amounts of the nanocarriers were measured by ICP-MS in Figure 5b. Without NIR irradiation, the resistance of PEG corona to nonspecific adsorption caused fairly low cellular uptake in the five cell lines. Once exposed under NIR irradiation, the nanocarriers presented preferred accumulations in the $\alpha_v\beta_3^+$ cells with the conversion of surface functional moieties from PEG to RGD; as controls, inhibiting the cells with RGD molecules efficiently prevented the nanocarriers from internalization into all the five cells, implying the key role of RGD shell in the recognition between the nanocarriers and the target cells. More importantly, even among the $\alpha_v\beta_3^+$ cells, it is feasible to enlarge the uptake distinction by switching the surface composition with NIR laser, leading to exclusive accumulation in targeted HeLa cells rather than normal NIH 3T3 cells. On the other hand, the cytotoxicity of the nanocarriers to cells could be further manipulated by controlling release rates, which were highly dependent on the abundance of the endogenous miRNAs. As a proof of concept, we chose miR-21 as a model trigger, which was significantly overexpressed in a wide variety of cancers, including glioblastoma, breast, lung, pancreas, liver, cervical, and various hematopoietic cancers.[46] Thus, by virtue of the differential expressions in integrin $\alpha_v\beta_3$ and miR-21 (Figure 5c), significant differences in cargo release were observed in the five cells under NIR irradiation (Figures 5a and S18), presenting massive released Dox and siRNAs in tumor cells; especially, even though relatively small amounts of nanocarriers were accumulated in MCF-7 cells, considerable cargo release

DOI: 10.1021/acsnano.5b08145
ACS Nano 2016, 10, 3637−3647

was still observed in the confocal and flow cytometric results due to the overexpressed miR-21. In this manner, the distinction in gene silence (Figure S19) and cell mortality (Figure 5d) among different cells was greatly enlarged, which was beneficial to maximize therapy efficacy and minimize side effects.

NIR-Guided Tumor Targeting and Antitumor Efficacy of D/R/SNCs *In Vivo*. First, to achieve the maximum therapeutic efficacy *in vivo*, the NIR laser power was optimized in a mouse xenograft tumor model. By subcutaneously injecting the nanocarriers around the tumor on the mice, as shown in Figure S20, more than 70% of the injected nanocarriers were internalized into the tumor cells at the power density between 0.5 to 1.0 W cm^{-2}, due to the exposure of $P43_{RGD}$. With the further increase of power density, the surface state around the nanocarriers was dominated by the DNA nanostructures with the shrinkage of $P43_{RGD}$, leading to the reduction of cellular uptake. Thus, to finely guide the specific cellular uptake, at 0.5, 1, 2, 4, and 6 h after the intravenous injection of the nanocarriers, the tumors on the mice were exposed under the 808 nm laser at 0.5 W cm^{-2} for 10 min; in the following 6 days, the tumors were irradiated for three times every 2 days, at each time the tumors were irradiated at 0.5 W cm^{-2} for 10 min for further cellular uptake and subsequently at 1.2 W cm^{-2} for 20 min for drug release. Then, the pharmacokinetic of the nanocarriers was assessed by detecting the gold and Dox amounts in the plasma after intravenous injection of different formulations (Figure S21). By virtue of PEG protection, D/R/SNCs displayed lower clearance (CL), longer half-time ($t_{1/2}$), and mean residence time (MRT), as well as excellent resistance to degradation, thereby reinforcing their retention in the tumor tissues. Thereafter, the *in vivo* biodistribution of D/R/SNCs was investigated to evaluate their tumor targeting capability under the NIR guidance. At day 1 and day 14 postinjection, the mice were euthanized, and the tumors as well as the normal organs were harvested for *ex vivo* imaging (Figure 6a) and ICP-MS analysis (Figure 6b). At day 1, the gold contents in the tumors were comparable to those in liver and kidney, indicating the passive accumulation of D/R/SNCs at tumor sites *via* EPR effect. Under the NIR irradiation, the internalization of the nanocarriers in tumor cells *via* receptor-mediated endocytosis and release of the siPLK1 and Dox in the presence of intracellular miRNA and ATP contributed to the strong fluorescence in the *ex vivo* imaging. In comparison, no fluorescence signal was detected in the unirradiated tumor and normal tissues even though massive nanocarriers were distributed in liver and kidney, suggesting that Dox leakage was efficiently prevented because the PEG coating has efficiently protected the nanocarriers against nuclease degradation and nonspecific uptake. After 14 days, guided by the NIR laser, the smart nanocarriers selectively entered the tumor cells and efficiently released the loaded siPLK1 and Dox, presenting a 4.5-fold gold content and strong fluorescence compared with the unirradiated mice, whereas the most of nanocarriers trapped in the normal organs were completely excreted with minute Dox leakage. As shown in Figures 6c and d, fast tumor growth was observed in the group of SNCs, indicating that the mild NIR irradiation at 0.5 W cm^{-2} exerted slight photothermal damage to the tumor cells; however, the simultaneous delivery of siPLK1 and Dox significantly inhibited the tumor growth compared with the control groups, especially with the mice treated with a high dosage of Dox solution. Furthermore, the tumor tissues were investigated by histological analysis stained by hematoxylin and eosin (HE) and apoptosis detection using terminal deoxynucleotidyl transferase dUTP nick end labeling (TUNEL) assay. As shown in Figure 6f, massive cell remission and high cell apoptosis occurred in the tumor treated with D/R/SNCs under NIR irradiation, confirming the synergistic effect for suppressing the tumor growth. On the other hand, the body weights of all the mice had no obvious changes during the treatment (Figure 6e); in particular, no pathological abnormality was observed from the HE staining images (Figure 6g) in heart, liver, spleen, and kidney of the mice treated with the nanocarriers, which was attributed to their low retention and zero premature leakage in the normal organs. Finally, it should be noted that multiple NIR irradiations utilized in the treatment could maximize the cellular uptake during the gradual passive accumulation of the nanocarriers at the tumor sites, and make the best of trace intracellular miRNAs, thus generating high release efficiency, continuous tumor inhibition, and minute side effect to normal tissues. Thus, the switchable PEG corona has successfully made the D/R/SNCs stealthy during the blood circulation, eliminated the nonspecific uptake by normal organs, and facilitated the passive accumulation at tumor sites, where specific cellular uptake and efficient release were achieved under the guidance of NIR laser, resulting in effective inhibition to tumor growth and minute side effect to normal tissues. Different from the thermal ablation in traditional photothermal therapy, more gentle NIR laser was employed in our strategy to precisely control the temperature in sequence as 39 and 43 °C. The excellent therapeutic efficacy of the nanocarriers inspired us to apply in mouse orthotopic transplantation tumor models in the future, providing a promising tool for clinical treatment in human patients.

CONCLUSIONS

In conclusion, we developed the smart nanocarriers consisting of gold nanorods as photothermal controllers, thermosensitive polymers as navigators, and Y-motifs as DNA nanorobots to realize the targeted delivery and controlled release of siRNA and Dox *in vivo*. The switchable surface of the smart nanocarriers successfully made the D/R/SNCs stealthy during blood circulation, eliminated the nonspecific uptake by normal organs and facilitated the passive accumulation at tumor sites, where specific cellular uptake were achieved under the guidance of NIR laser. Followed by controlled release of siRNA and Dox in the presence of miRNAs/ATP, synergetic inhibition to tumor growth and minute side effect to normal tissues were detected in the tumor-bearing mice. With the development of DNA nanotechnology, particularly in aptamer screening and DNA origami, multifunctional DNA nanostructures responsive to exclusive intracellular stimuli can be designed, providing smarter nanodevices that work like viruses for the personalized treatment of human disease with gene and drugs.[47]

MATERIALS AND METHODS

Materials. All chemicals were listed in Supporting Information and used as received. All aqueous solutions were prepared using DEPC treated ultrapure water from a Milli-Q system (Millipore, U.S.A.). The DNA sequences containing RNA nucleotides were purchased from Takara Biotechnology Co. Ltd. (Dalian, China). The other DNA oligonucleotide sequences were purchased from Shanghai Sangon Biological Engineering Technology & Services Co. (Shanghai, China). The microRNA sequences were obtained from Shanghai

DOI: 10.1021/acsnano.5b08145
ACS Nano 2016, 10, 3637−3647

GenePharma (Shanghai, China). The oligonucleotide sequences for preparing nanoprobes in Figure 2a: Y_a (5′-CGTACTATCAGGCAAGCTACTTACCTGGGGGAGTATTGCGGAGGAAGGTTCAACATCAGTCTGATAGTACG$_{FAM}$-3′); Y_b (5′-CACGGCGAATGACTCGTACCTTCCTCCGCAATACTCCCCC-3′); Y_c (5′-$_{BHQ}$TCGACTATCAGACTGATCATTCGCCGTG-3′).

The oligonucleotide sequences for preparing D/R/SNCs in Figure 4: Y_a (5′-CGTACTATCAGGCAAGCTACTTACCTGGGGGAGTATTGCGGAGGAAGGTTCAACATCAGTCTGATAGTACG-3′); Y_c (5′-TCGACTATCAGACTGATCATTCGCCGTG-3′). siRNA coupled Y_b:

siPLK1-1-s (5′-UGAAGAAGAUCACCCUCCUUATT-3′); siPLK1-1-as (5′-UAAGGAGGGUGAUCUUCUUCATTCACGGCGAATGACTCGTACCTTCCTCCGCAATACTCCCCC$_{FAM}$-3′); siPLK1-2-s (5′-UGAAGAAGAUCACCCUCCUUATTCACGGCGAATGACTCGTACCTTCCTCCGCAATACTCCCCC$_{FAM}$-3′); siPLK1-2-as (5′-UAAGGAGGGUGAUCUUCUUCATT-3′).

Preparation of the Smart Nanocarriers D/R/SNCs. First, gold nanorods (GRs) and thermosensitive polymers were prepared. The GRs with exceptional monodispersity and tunable longitudinal surface plasmon resonances were synthesized and overgrown according to the published protocol.[45,46] Bipolymer of pNIPAAm-*co*-pAAm terminated with PEG ($P39_{PEG}$) and terpolymer of pNIPAAm-*co*-pAAm-*co*-pHEAAm conjugated with multiple RGD peptides ($P43_{RGD}$) were synthesized *via* atom transfer radical polymerization and functionalized *via* copper(I)-catalyzed azide−alkyne cycloaddition (CuAAC).

In a typical synthesis of D/R/SNCs, thiolated anchor-DNA (4 OD) was deprotected in distilled water (500 μL) containing 5 mM TCEP. After incubation at room temperature for 3 h, 200 μL of GRs (25 nM) was added into the solution, which was shaken for 1 h until 5 × TBE (100 μL), $P39_{PEG}$ (80 μL), and $P43_{RGD}$ (20 μL) were added with a final molar ratio of 2:1:3 ($P39_{PEG}$:$P43_{RGD}$:anchor-DNA). Then the mixture was gently shaken for 24 h. NaCl solution was slowly added into the colloidal particle solutions to age overnight. The A/SNCs were obtained by repeated centrifugation and washing. Then, the Y-motifs were loaded on A/SNCs to obtain R/SNCs as follows: after the siPLK1-1-s and siPLK1-1-as with the molar ratio of 1:1 were incubated for 30 min, stoichiometric amounts of strands Y_a, siPLK1-1 coupled Y_b, and Y_c were mixed in Tris−HCl buffer; the mixture was incubated at 95 °C for 5 min, and then sequentially cooled down to 65 °C, 60 °C, 55 °C, 50 °C, and 45 °C (each step for 5 min). Then, the mixture was added into the A/SNCs, which had been preheated to 45 °C, and further incubated for 1 h. Finally, the obtained R/SNCs (200 μL, 10 nM) were shaken with Dox stock solution (200 μL, 2.5 mM) for 6 h. The resulting D/R/SNCs were purified by centrifugation. More detailed procedures were stated in Supporting Information.

Cell Culture. HeLa, NIH 3T3, HEK 293T, MCF-7, and A549 were obtained from the Institute of Cell Biology at the Chinese Academy of Sciences (Shanghai, P. R. China) and cultured in DMEM (Life Technologies, Grand Island, NY, U.S.A.) at 37 °C under 5% CO_2 atmosphere, supplemented with L-glutamine (2 mM) and 10% fetal bovine serum (FBS). At the logarithmic growth phase, the cells were incubated with different nanocarriers in cultured medium.

Cellular Uptake, Intracellular Trafficking, and Simultaneous Release of D/R/SNCs *In Vitro*. The NIR-guided uptake and miRNA-triggered release of D/R/SNCs nanocarriers were generally performed as follows: the cells were incubated with the cultured medium containing nanocarriers under NIR irradiation for 10 min every 20 min; after 2 h, the cells were cultured in fresh medium for another 2 h, during which time the cells were exposed upon the NIR irradiation for 10 min every 20 min. To minimize the damage to the cells caused by NIR irradiation, all the NIR irradiation was performed as follows: expose the cells at NIR light for 30 s and remove the NIR light for 30 s, then repeat the procedure for 10 min. The amounts of the nanocarriers internalized into the cells were evaluated by using inductively coupled plasma mass spectrometry (ICP-MS, Thermo Fisher) according to a published protocol.[47] The intracellular trafficking, simultaneous release of the FAM labeled siRNA and Dox could be visualized by confocal images and flow cytometry.

***In Vitro* Controlled Release by Adjusting NIR Power, miRNA Level, and ATP Concentration.** The effects of NIR power on cell uptake and drug release were investigated by exposing the cells under NIR light at different power densities. The release rates were reflected by the fluorescence intensities of the released dox measured by CLSM and flow cytometry. The intracellular miRNA expressions were modulated by transfecting miRNA mimics or antisense strands into the cells. Cell transfection was performed following a standard protocol using Lipofectamine 2000 (Invitrogen, U.S.A.). The intracellular ATP levels were adjusted by incubating with IAA to inhibit the ATP production in the cells. The content of ATP in cells was determined by ATPlite Assay Kit (PerkinElmer, U.S.A.) according to the proposed protocol.

Therapeutic Efficacy *In Vitro*. Cytotoxicity of the nanocarriers was assessed through cell viability by MTT (3-(4,5-dimethylthiazol-2-yl)-2,5-diphenyltetrazolium bromide) assay. Apoptosis of HeLa cells after treated with nanocarriers was detected using Annexin V-FITC Apoptosis Detection Kit (Dojindo Molecular Technologies, Inc., Kumamoto, Japan). To evaluate the transfection effect, the cellular levels of PLK1 mRNA and protein were assessed using quantitative real-time PCR (qRT-PCR) and Western blotting, respectively. The cells were seeded in six-well tissue culture plates at 2×10^5 cells/well and incubated at 37 °C in 5% CO_2 for 24 h to reach ∼70% confluence. Different nanocarriers were added and incubated with the cells for 24 h (for RNA isolation) and 48 h (for protein extraction).

***In Vivo* Antitumor Efficacy.** All animals had free access to rodent chow and water. The experiments were conducted according to the use and care guidelines of the experimental animals of Jiangsu Province, P. R. China. To set up a tumor xenograft mouse model, the female nude mice (6 weeks) were subcutaneously inoculated in the second right mammary fat pad with 1×10^7 HeLa cells. The tumor size was monitored by a vernier caliper and the tumor volume was calculated as $V = (L \times W^2)/2$, where L and W were the length and width of the tumor, respectively. When the tumor volumes reached to 50 mm^3, the tumor-bearing mice were weighed and randomly divided into five groups ($n = 5$). From here on, the mice were intravenously injected with (i) PBS as negative control, (ii) Dox solution (1 mg kg^{-1}), (iii) D/R/SNCs with NIR irradiation (20 mg kg^{-1}), (iv) D/R/SNCs without NIR irradiation (20 mg kg^{-1}), and (v) SNCs with NIR irradiation (20 mg kg^{-1}). In group iii and v, at 0.5, 1, 2, 4, and 6 h after the intravenous injection of the nanocarriers, the tumors on the mice were exposed under the 808 nm laser at 0.5 W cm^{-2} for 10 min; in

DOI: 10.1021/acsnano.5b08145
ACS Nano 2016, 10, 3637−3647

the following 6 days, the tumors were irradiated three times every 2 days; at each time, the tumors were irradiated at 0.5 W cm^{-2} for 10 min and subsequently at 1.2 W cm^{-2} for 20 min. The tumor size and the weight of the mice were measured every 2 days. At Day 14, all the mice were euthanized, and the major organs including tumor, heart, liver, spleen, lung, and kidney were collected, washed with cold PBS, and fixed in the 10% neutral-buffered formalin. For the hematoxylin and eosin staining, the formalin-fixed organs were embedded in paraffin blocks and visualized by optical microscope (Olympus IX51, Japan). For the TUNEL apoptosis staining, the fixed tumor sections were stained by the TUNEL Cell Death Detection Kit (KGA702, KeyGen, China) according to the manufacturer's protocol and visualized by optical microscope.

Statistic Analysis. Data were presented as mean ± standard deviation (SD). Student's *t*-test was applied to test the significance of the difference, which was considered to be significant when $p < 0.05$ (*) and very significant when $p < 0.01$ (**).

ASSOCIATED CONTENT

Supporting Information

The Supporting Information is available free of charge on the ACS Publications website at DOI: 10.1021/acsnano.5b08145.

Chemicals, DNA and RNA sequences, detailed experiment procedures, characterization of the nanocarriers, the evaluation of the specificity, efficiency, and stability of the drug nanocarriers (Figures S1–S21). (PDF)

AUTHOR INFORMATION

Corresponding Authors

*E-mail: jjzhu@nju.edu.cn.
*E-mail: jnchen@nju.edu.cn.
*E-mail: minqianhao@nju.edu.cn.

Author Contributions

§These authors contributed equally to this work.

Notes

The authors declare no competing financial interest.

ACKNOWLEDGMENTS

This research was supported by National Natural Science Foundation of China (Nos.: 21335004, 21327902, 21427807, 31571458) and National Basic Research Program of China (2011CB933502, 2012CB517603). P.Z. also thanks the support from the Program A for Outstanding Ph.D. Candidate of Nanjing University.

REFERENCES

(1) Leung, S. J.; Romanowski, M. NIR-Activated Content Release from Plasmon Resonant Liposomes for Probing Single-Cell Responses. *ACS Nano* **2012**, *6*, 9383–9391.

(2) Hong, B. J.; Chipre, A. J.; Nguyen, S. T. Acid-Degradable Polymer-Caged Lipoplex (PCL) Platform for siRNA Delivery: Facile Cellular Triggered Release of siRNA. *J. Am. Chem. Soc.* **2013**, *135*, 17655–17658.

(3) Li, W.; Wang, J.; Ren, J.; Qu, X. Near-Infrared- and pH-Responsive System for Reversible Cell Adhesion Using Graphene/Gold Nanorods Functionalized with i-motif DNA. *Angew. Chem., Int. Ed.* **2013**, *52*, 6726–6730.

(4) Nam, J.; La, W.-G.; Hwang, S.; Ha, Y. S.; Park, N.; Won, N.; Jung, S.; Bhang, S. H.; Ma, Y.-J.; Cho, Y.-M.; et al. pH-Responsive Assembly of Gold Nanoparticles and "Spatiotemporally Concerted" Drug Release for Synergistic Cancer Therapy. *ACS Nano* **2013**, *7*, 3388–3402.

(5) Zhang, Z.; Balogh, D.; Wang, F.; Sung, S. Y.; Nechushtai, R.; Willner, I. Biocatalytic Release of an Anticancer Drug from Nucleic-Acids-Capped Mesoporous SiO2 Using DNA or Molecular Biomarkers as Triggering Stimuli. *ACS Nano* **2013**, *7*, 8455–8468.

(6) Tarn, D.; Ashley, C. E.; Xue, M.; Carnes, E. C.; Zink, J. I.; Brinker, C. J. Mesoporous Silica Nanoparticle Nanocarriers: Biofunctionality and Biocompatibility. *Acc. Chem. Res.* **2013**, *46*, 792–801.

(7) Zhang, Z.; Wang, J.; Nie, X.; Wen, T.; Ji, Y.; Wu, X.; Zhao, Y.; Chen, C. Near Infrared Laser-Induced Targeted Cancer Therapy Using Thermoresponsive Polymer Encapsulated Gold Nanorods. *J. Am. Chem. Soc.* **2014**, *136*, 7317–7326.

(8) Dai, Y.; Xiao, H.; Liu, J.; Yuan, Q.; Ma, P. A.; Yang, D.; Li, C.; Cheng, Z.; Hou, Z.; Yang, P.; et al. *In Vivo* Multimodality Imaging and Cancer Therapy by Near-Infrared Light-Triggered Trans-Platinum Pro-Drug-Conjugated Upconverison Nanoparticles. *J. Am. Chem. Soc.* **2013**, *135*, 18920–18929.

(9) Nair, M.; Guduru, R.; Liang, P.; Hong, J.; Sagar, V.; Khizroev, S. Externally Controlled on-Demand Release of Anti-HIV Drug Using Magneto-Electric Nanoparticles as Carriers. *Nat. Commun.* **2013**, *4*, 1707.

(10) Liang, X.; Gao, J.; Jiang, L.; Luo, J.; Jing, L.; Li, X.; Jin, Y.; Dai, Z. Nanohybrid Liposomal Cerasomes with Good Physiological Stability and Rapid Temperature Responsiveness for High Intensity Focused Ultrasound Triggered Local Chemotherapy of Cancer. *ACS Nano* **2015**, *9*, 1280–1293.

(11) Ling, D.; Park, W.; Park, S.-j.; Lu, Y.; Kim, K. S.; Hackett, M. J.; Kim, B. H.; Yim, H.; Jeon, Y. S.; Na, K.; et al. Multifunctional Tumor pH-Sensitive Self-Assembled Nanoparticles for Bimodal Imaging and Treatment of Resistant Heterogeneous Tumors. *J. Am. Chem. Soc.* **2014**, *136*, 5647–5655.

(12) Stephen, Z. R.; Kievit, F. M.; Veiseh, O.; Chiarelli, P. A.; Fang, C.; Wang, K.; Hatzinger, S. J.; Ellenbogen, R. G.; Silber, J. R.; Zhang, M. Redox-Responsive Magnetic Nanoparticle for Targeted Convection-Enhanced Delivery of O6-Benzylguanine to Brain Tumors. *ACS Nano* **2014**, *8*, 10383–10395.

(13) Zhang, J.; Yuan, Z. F.; Wang, Y.; Chen, W. H.; Luo, G. F.; Cheng, S. X.; Zhuo, R. X.; Zhang, X. Z. Multifunctional Envelope-Type Mesoporous Silica Nanoparticles for Tumor-Triggered Targeting Drug Delivery. *J. Am. Chem. Soc.* **2013**, *135*, 5068–5073.

(14) Mo, R.; Jiang, T.; DiSanto, R.; Tai, W.; Gu, Z. ATP-Triggered Anticancer Drug Delivery. *Nat. Commun.* **2014**, *5*, 3364.

(15) Di Leva, G.; Garofalo, M.; Croce, C. M. MicroRNAs in Cancer. *Annu. Rev. Pathol.: Mech. Dis.* **2014**, *9*, 287–314.

(16) Bartel, D. P. MicroRNAs: Genomics, Biogenesis, Mechanism, and Function. *Cell* **2004**, *116*, 281–297.

(17) Zhang, P.; Cheng, F.; Zhou, R.; Cao, J.; Li, J.; Burda, C.; Min, Q.; Zhu, J.-J. DNA-Hybrid-Gated Multifunctional Mesoporous Silica Nanocarriers for Dual-Targeted and MicroRNA-Responsive Controlled Drug Delivery. *Angew. Chem., Int. Ed.* **2014**, *53*, 2371–2375.

(18) Dong, H.; Lei, J.; Ding, L.; Wen, Y.; Ju, H.; Zhang, X. MicroRNA: Function, Detection, and Bioanalysis. *Chem. Rev.* **2013**, *113*, 6207–6233.

(19) Zhang, P.; He, Z.; Wang, C.; Chen, J.; Zhao, J.; Zhu, X.; Li, C.-Z.; Min, Q.; Zhu, J.-J. *In Situ* Amplification of Intracellular MicroRNA with MNAzyme Nanodevices for Multiplexed Imaging, Logic Operation, and Controlled Drug Release. *ACS Nano* **2015**, *9*, 789–798.

(20) Prusty, D. K.; Kwak, M.; Wildeman, J.; Herrmann, A. Modular Assembly of a Pd Catalyst within a DNA Scaffold for the Amplified Colorimetric and Fluorimetric Detection of Nucleic Acids. *Angew. Chem., Int. Ed.* **2012**, *51*, 11894–11898.

(21) Liu, G.; Wan, Y.; Gau, V.; Zhang, J.; Wang, L.; Song, S.; Fan, C. An Enzyme-Based E-DNA Sensor for Sequence-Specific Detection of Femtomolar DNA Targets. *J. Am. Chem. Soc.* **2008**, *130*, 6820–6825.

(22) Liu, S.; Wang, C.; Zhang, C.; Wang, Y.; Tang, B. Label-Free and Ultrasensitive Electrochemical Detection of Nucleic Acids Based on

DOI: 10.1021/acsnano.5b08145
ACS Nano 2016, 10, 3637–3647

Autocatalytic and Exonuclease III-Assisted Target Recycling Strategy. *Anal. Chem.* **2013**, *85*, 2282−2288.
(23) Freeman, R.; Liu, X.; Willner, I. Amplified Multiplexed Analysis of DNA by the Exonuclease III-Catalyzed Regeneration of the Target DNA in the Presence of Functionalized Semiconductor Quantum Dots. *Nano Lett.* **2011**, *11*, 4456−4461.
(24) Wang, F.; Liu, X.; Willner, I. DNA Switches: From Principles to Applications. *Angew. Chem., Int. Ed.* **2015**, *54*, 1098−1129.
(25) Tang, W.; Wang, H.; Wang, D.; Zhao, Y.; Li, N.; Liu, F. DNA Tetraplexes-Based Toehold Activation for Controllable DNA Strand Displacement Reactions. *J. Am. Chem. Soc.* **2013**, *135*, 13628−13631.
(26) Gottesman, M. M. Mechanisms of Cancer Drug Resistance. *Annu. Rev. Med.* **2002**, *53*, 615−627.
(27) Creixell, M.; Peppas, N. A. Co-Delivery of siRNA and Therapeutic Agents Using Nanocarriers to Overcome Cancer Resistance. *Nano Today* **2012**, *7*, 367−379.
(28) Williford, J.-M.; Wu, J.; Ren, Y.; Archang, M. M.; Leong, K. W.; Mao, H.-Q. Recent Advances in Nanoparticle-Mediated siRNA Delivery. *Annu. Rev. Biomed. Eng.* **2014**, *16*, 347−370.
(29) Kanasty, R.; Dorkin, J. R.; Vegas, A.; Anderson, D. Delivery Materials for siRNA Therapeutics. *Nat. Mater.* **2013**, *12*, 967−977.
(30) Yang, X.-Z.; Du, J.-Z.; Dou, S.; Mao, C.-Q.; Long, H.-Y.; Wang, J. Sheddable Ternary Nanoparticles for Tumor Acidity-Targeted siRNA Delivery. *ACS Nano* **2012**, *6*, 771−781.
(31) Hatakeyama, H.; Akita, H.; Ito, E.; Hayashi, Y.; Oishi, M.; Nagasaki, Y.; Danev, R.; Nagayama, K.; Kaji, N.; Kikuchi, H.; et al. Systemic Delivery of siRNA to Tumors Using a Lipid Nanoparticle Containing a Tumor-Specific Cleavable PEG-Lipid. *Biomaterials* **2011**, *32*, 4306−4316.
(32) Perche, F.; Biswas, S.; Wang, T.; Zhu, L.; Torchilin, V. P. Hypoxia-Targeted siRNA Delivery. *Angew. Chem., Int. Ed.* **2014**, *53*, 3362−3366.
(33) Zhang, K.; Zhu, X.; Jia, F.; Auyeung, E.; Mirkin, C. A. Temperature-Activated Nucleic Acid Nanostructures. *J. Am. Chem. Soc.* **2013**, *135*, 14102−14105.
(34) Barhoumi, A.; Wang, W.; Zurakowski, D.; Langer, R. S.; Kohane, D. S. Photothermally Targeted Thermosensitive Polymer-Masked Nanoparticles. *Nano Lett.* **2014**, *14*, 3697−3701.
(35) Morlieras, J.; Dufort, S.; Sancey, L.; Truillet, C.; Mignot, A.; Rossetti, F.; Dentamaro, M.; Laurent, S.; Vander Elst, L.; Muller, R. N.; et al. Functionalization of Small Rigid Platforms with Cyclic RGD Peptides for Targeting Tumors Overexpressing $\alpha v\beta 3$-Integrins. *Bioconjugate Chem.* **2013**, *24*, 1584−1597.
(36) Biswas, S.; Kinbara, K.; Niwa, T.; Taguchi, H.; Ishii, N.; Watanabe, S.; Miyata, K.; Kataoka, K.; Aida, T. Biomolecular Robotics for Chemomechanically Driven Guest Delivery Fuelled by Intracellular ATP. *Nat. Chem.* **2013**, *5*, 613−620.
(37) Wang, F.; Lu, C.-H.; Willner, I. From Cascaded Catalytic Nucleic Acids to Enzyme−DNA Nanostructures: Controlling Reactivity, Sensing, Logic Operations, and Assembly of Complex Structures. *Chem. Rev.* **2014**, *114*, 2881−2941.
(38) Zhou, T.; Chen, P.; Niu, L.; Jin, J.; Liang, D.; Li, Z.; Yang, Z.; Liu, D. pH-Responsive Size-Tunable Self-Assembled DNA Dendrimers. *Angew. Chem., Int. Ed.* **2012**, *51*, 11271−11274.
(39) Xiao, Z.; Ji, C.; Shi, J.; Pridgen, E. M.; Frieder, J.; Wu, J.; Farokhzad, O. C. DNA Self-Assembly of Targeted Near-Infrared-Responsive Gold Nanoparticles for Cancer Thermo-Chemotherapy. *Angew. Chem., Int. Ed.* **2012**, *51*, 11853−11857.
(40) Sun, T.-M.; Du, J.-Z.; Yao, Y.-D.; Mao, C.-Q.; Dou, S.; Huang, S.-Y.; Zhang, P.-Z.; Leong, K. W.; Song, E.-W.; Wang, J. Simultaneous Delivery of siRNA and Paclitaxel *via* a "Two-in-One" Micelleplex Promotes Synergistic Tumor Suppression. *ACS Nano* **2011**, *5*, 1483−1494.
(41) Huschka, R.; Barhoumi, A.; Liu, Q.; Roth, J. A.; Ji, L.; Halas, N. J. Gene Silencing by Gold Nanoshell- Mediated Delivery and Laser-Triggered Release of Antisense Oligonucleotide and siRNA. *ACS Nano* **2012**, *6*, 7681−7691.
(42) Chou, T.-C. Drug Combination Studies and Their Synergy Quantification Using the Chou-Talalay Method. *Cancer Res.* **2010**, *70*, 440−446.
(43) Ye, Y.; Chen, X. Integrin Targeting for Tumor Optical Imaging. *Theranostics* **2011**, *1*, 102−126.
(44) Achilefu, S.; Bloch, S.; Markiewicz, M. A.; Zhong, T.; Ye, Y.; Dorshow, R. B.; Chance, B.; Liang, K. Synergistic Effects of Light-Emitting Probes and Peptides for Targeting and Monitoring Integrin Expression. *Proc. Natl. Acad. Sci. U. S. A.* **2005**, *102*, 7976−7981.
(45) Hölig, P.; Bach, M.; Völkel, T.; Nahde, T.; Hoffmann, S.; Müller, R.; Kontermann, R. E. Novel RGD Lipopeptides for the Targeting of Liposomes to Integrin-Expressing Endothelial and Melanoma Cells. *Protein Eng., Des. Sel.* **2004**, *17*, 433−441.
(46) Krichevsky, A. M.; Gabriely, G. miR-21: A Small Multi-Faceted RNA. *J. Cell. Mol. Med.* **2009**, *13*, 39−53.
(47) Pei, H.; Zuo, X.; Zhu, D.; Huang, Q.; Fan, C. Functional DNA Nanostructures for Theranostic Applications. *Acc. Chem. Res.* **2014**, *47*, 550−559.

DOI: 10.1021/acsnano.5b08145
ACS Nano 2016, 10, 3637−3647